Growth of single-crystal imine-linked covalent organic frameworks in water using amphiphilic amino-acid derivatives

Zhipeng Zhou
Sun Yat-sen University
Lei Zhang
Peking University
Yonghang Yang
Sun Yat-sen University
Iñigo J. Vitorica-Yrezabal
The University of Manchester
Honglei Wang
Sun Yat-sen University
Fanglin Tan
Sun Yat-sen University
Li Gong
Sun Yat-sen University
Yuyao Li
Sun Yat-sen University
Pohua Chen
Peking University
Xin Dong
Sun Yat-sen University
Zihao Liang
Sun Yat-sen University
Jing Yang
Sun Yat-sen University
Chao Wang
Sun Yat-sen University
Yuexian Hong
Sun Yat-sen University
Yi Qiu
Peking University
Armin Gölzhäuser

Bielefeld University
Xudong Chen
Sun Yat-sen University
Haoyuan Qi
Universität Ulm
Sihai Yang
he University of Manchester
Wei Liu
Sun Yat-sen University
Junliang Sun
Peking University
Zhikun Zheng (zhengzhikun@mail.sysu.edu.cn)
Sun Yat-sen University

Research Article

Keywords: Covalent organic frameworks, single crystal

Posted Date: March 16th, 2023

DOI: https://doi.org/10.21203/rs.3.rs-2696940/v1

Abstract

Living organisms explored functional biomolecules such as proteins bearing glycine to create single-crystals of minerals in water without resorting to low levels of supersaturation. However, this strategy remains poorly effective in the crystallization of organic polymers. Here, we report a biomimetic strategy and its implementation to synthesize single-crystals of an important class of organic polymers - covalent organic frameworks (COFs) in water under ambient conditions. The strategy explores assemblies of amphiphilic molecules of glycine derivatives as dynamic barriers to separate monomers in water and oil phases, thereby regulating the polymerization and crystallization processes. Monomers first polymerized into disordered solids regardless of concentration variations over five orders of magnitude, then transformed into crystals in a step-by-step fashion with monomers and dimers as main building units, affording six types of single-crystals at the gram-scale with yields of ≥ 92% besides a two-dimensional COF-366. This study will be a valuable addition to the repertoire of crystallization path and methodology of organic polymers and promote their industrial applications.

Full Text

Living organisms synthesize single crystals of biominerals through controlled nucleation and growth assisted by functional biomolecules such as proteins bearing glycine in water at near room temperature[1,2]. The crystallization process typically involves the sequestering and concentrating of ions from water within a matrix or compartment, in which a family of disordered solid precursors are formed, accumulated, stabilized, temporarily stored, and further utilized as starting materials for crystallization without resorting to low levels of supersaturation[3-5]. Adapting the biomineralization path to synthesize crystals with high production efficiency and structure diversity remains challenging. Here, we mimic this strategy to synthesize single crystals of an important class of organic materials - covalent organic frameworks (COFs) in water under ambient conditions.

COFs, constructed from organic monomers termed as knots and linkers through covalent bonds, are polymeric materials with permanent porosity[6]. Their synthesis typically involves volatile organic solvents, high temperature, high pressure and inert atmosphere or vacuum[7,8]. During the synthesis, amorphous polymeric materials forms spontaneously, aggregates and precipitates rapidly, and depends on random error-corrections offered by microscopic reversibility of the dynamic covalent bonds to crystallize into network structures[9]. The free polymerization and crystallization process naturally requires trial and error, chemical intuition and large-scale screening to find an experimental condition to crystallize a specific structure[10], and prevents the formation of single crystal COFs with controlled size and their large-scale synthesis[11,12].

Our strategy to creating single-crystal COFs explores amphiphilic molecules of palmitoylglycine (C_{16}-GlyA) with long hydrophobic chains as dynamic barriers to separate knots and linkers in water and oil phases (C_{16}-GlyA phase) to regulate the polymerization and crystallization processes (Fig. 1a, b, c). C_{16}-

GlyA was synthesized from palmitoyl chloride and glycine (see Supplementary Information Section 1.1 for details). It can assemble into vesicles with a layered supramolecular structure of around 331 nm in water (Extended Data Fig. 1a, b), affording a hydrophobic compartment[13].

We started with COF-301 that was in previous work only obtained as poorly crystalline aggregates with a low yield and no structure elucidation could be enabled despite of its high promise in different areas[14, 15] by condensation of 2,5-dihydroxy-1,4-benzenedicarboxaldehyde (linker-A) with one equivalent of tetrakis(4-aminophenyl)methane (TAM) under ambient conditions. Solution nuclear magnetic resonance (NMR) and electrospray ionization high-resolution mass spectrometry indicated that TAM protonated with *p*-toluenesulfonic acid (PTSA) mainly dissolved in water while linker-A was in the C_{16}-GlyA phase when added individually (Extended Data Fig. 1a, b and Extended Data Fig. 2). When powders of linker-A were added into the C_{16}-GlyA emulsion, it tuned from white to yellow. The size of vesicles grew to ~ 503 nm and no precipitate or vesicles of other size was detected (Extended Data Fig. 1a), furthering confirming the dissolution of the monomer in the C_{16}-GlyA phase. Subsequent addition of PTSA-protonated TAM led to gel-like mixtures within 10 minutes. After thorough rinsing with water and tetrahydrofuran, disordered solid phase with a yield of 91% was obtained (Fig. 1d and Extended Data Fig. 3a, b). No monomers were detected in the solid phase by high-resolution mass spectrometry, and the broad differential thermal gravity (DTG) peak suggested existence of a mixture of materials (Fig. 2a), and Fourier transform infrared (FTIR) spectra indicated they were polyimines containing large amounts of free aldehyde groups (Extended Data Fig. 3c).

We then evaluated the yield and crystallinity of the isolated solid phase at different reaction time. The yield showed no obvious time dependence and fluctuated between 91% and 95% (Fig. 2b). Bragg peaks of (2 0 0), (2 1 1) and (1 1 4) of COF-301 emerged after two days and single-crystal COF-301 could be clearly observed by optical microscopy (Extended Data Fig. 3a and Fig. 2c), suggesting a gradual amorphous-to-crystalline transition. As the reaction proceeded, the intensities of Bragg peaks increased, demonstrating gradual transformation of the disordered phase to crystals (Fig. 2b and Extended Data Fig. 3a, b). As also visualized by optical microscopy (Fig. 2c), 2 μm-sized crystals occurred on day two and more appeared with the increase of time. Pure single-crystal COF-301 was obtained after 14 days (Fig. 1e). They are uniform cuboids with typical length and width of around 2 μm and 0.6 μm (length/width = 3.3) at a molar concentration of linker-A of 0.05 mol L^{-1}, respectively. Mono-dispersed crystals were obtained despite the variation of the concentration of the monomers by five orders of values from 0.005 mmol L^{-1} to 0.5 mol L^{-1}. Notably, the size of the crystal increased from ~ 0.6 μm × 0.08 μm at 0.005 mmol L^{-1} to ~ 20 μm × 10 μm at 0.5 mol L^{-1} (Fig. 1f, g). The increase of the crystal size with the increase of the concentrations of the reactants in solution is contrary to the correlation in normal crystal growth[16]. Meanwhile, policies such as the usage of poor solvent to decrease the solubility of reactants, addition of reaction inhibitors/competitors and slow addition of reactants were employed to keep low concentrations of reactants to decrease amorphous parts and increase crystal size of COFs in contemporary methods[10-12].

Transmission electron microscopy (TEM) revealed that there was ~ 30 nm of adsorbed layer on the surface of the crystals (Fig. 2d, left), which could be removed by rinsing with tetrahydrofuran (Fig. 2d, right). Characteristic peaks of C_{16}-GlyA in confocal Raman spectroscopy disappeared after rinsing, indicating the main component of the adsorbed layer was the amino-acid derivative (Extended Data Fig. 3d). Note that the weak interactions (mainly hydrophobic-hydrophobic and hydrogen bonding interactions) among C_{16}-GlyA were highly dynamic, which facilitated the diffusion of TAM and PTSA. Deprotonated TAMs entered the microenvironment and reacted with linker-A, trigging the nucleation and growth of the crystal, while PTSA-protonated TAMs diffused to water due to solubility (Extended Data Figs. 1 and 2).

We selected an as-synthesized COF-301 (termed as COF-301-S) to prove single crystallinity and resolve the atomic structure with single-crystal XRD (see Supplementary Information Section 2 for details). COF-301-S was single crystal with a tetragonal space group of $I4_1/a$ (a = 26.434(4) Å, c = 7.5876(15) Å) and 7-fold interpenetration. The single network exhibits a diamond-type topology in which each TAM molecule is connected to four linker-As (Fig. 3a). The refined data resolution was ~ 0.9 Å, and all non-hydrogen atoms in the COF-301-S were identified. The selected area electron diffraction revealed that the interpenetration direction, *i.e.* along the longest diagonal of the unit cage (Fig. 2c and Fig. 3a, black arrow indicates the direction), was parallel to the elongation direction of the cuboids. The COF-301-S has one-dimensional (1D) straight channels along the interpenetration direction. A notable framework distortion was observed upon removal of C_{16}-GlyA by rinsing with tetrahydrofuran (Fig. 3b). The topology and interpenetration degree remained, while the pore size changed from 9.6 Å to 3.1 Å. The washed COF-301 (termed as COF-301-W) exhibited a different phase with a symmetry of $I2/c$ (a = 20.276(8) Å, b = 8.7098(18) Å, c = 20.212(4) Å, β = 99.308(12) °) (see Supplementary Information Section 3 for details).

We then investigated the surface morphology evolution of COF-301 to gain an insight into the crystal growth model. Intentionally aggregated crystals were prepared by dip coating on newly cleaved mica for characterization with atomic force microscopy (AFM). Disparate surface morphologies on the top and side facets of the cuboids have been observed (Fig. 2e, f). The (010) plane exhibits a higher density of growth sites or kinks than (100)/(001) planes (Fig. 2c, e and f), which is a characteristic of adhesive growth in which the building units stochastically integrate into the growing surface[17]. The (100)/(001) planes, on the other hand, show a train of terraces indicating layer-by-layer growth in which the building units preferentially integrate into the kink sites along the terrace edge (Fig. 2f). Due to the limited number of kink sites, the growth rate of the layer-by-layer mode is lower than that of the adhesive mode[18, 19], leading to growth anisotropy. The line scans in Fig. 2e present the typical step sizes on the top surface, in which 0.22 nm, *i.e.* the height difference between interpenetrated networks, and its multiples have been identified (Fig. 2g). The terrace height on the (100)/(001) facets has four typical values (Fig. 2f), *i.e.* 1.0 nm (one TAM + one linker-A), 1.3 nm (one TAM + two linker-A), 1.7 nm (two TAM + one linker-A), and 2.0 nm (two TAM + two linker-A) (Fig. 2h). The sub-unit-cell step heights on both the top and side facets suggest that monomers and dimers are the main fundamental building units during the crystal growth. The step-by-step crystal growth from solution involving disordered solids differs from known

crystallization path either from a saturated solution and or a melt in crystal growth[20]. It also differs from the error-correction mechanism found in contemporary synthesis methods for COFs and two-dimensional (2D) polymers[9, 21, 22].

To understand the effects of different parameters on the isolated yield of the solid phase and its conversion ratio to single-crystal COFs, the length of the hydrophobic chain of the amphiphilic molecules of amino-acid derivatives and their head groups and added catalysts were investigated. We first performed control experiments without C_{16}-GlyA, no solid was obtained even over a month. We then synthesized octanoylglycine (C_8-GlyA), decanoylglycine (C_{10}-GlyA), dodecanoylglycine (C_{12}-GlyA), tetradecanoylglycine (C_{14}-GlyA) and stearoylglycine (C_{18}-GlyA) (see Supplementary Information Section 1.1 for details) to investigate the effects of the length of the hydrophobic chain of the glycine derivatives (Extended Data Fig. 4a). Little solid was obtained for C_8-GlyA, C_{10}-GlyA, and C_{12}-GlyA, the yield of solid phase and crystals was 87% and 79% for C_{14}-GlyA, and then both reached maximum for C_{16}-GlyA. With C_{18}-GlyA, the yield of solid phase decreased to 79% (Extended Data Fig. 4a). The results indicated that the hydrophobicity and order of the assembled structure of the derivatives played important roles in regulating the diffusion, polymerization and crystallization process for the formation of COF-301. C_8-GlyA, C_{10}-GlyA, and C_{12}-GlyA were packed too loosely to form micelles, and therefore unable to regulate these processes[23]. With the increase of the chain length, and therefore the enhancement of the hydrophobicity and order of the assembled structures, larger micelles were formed and higher yields were achieved (Extended Data Fig. 1a). The hydrophobicity of C_{18}-GlyA hindered its efficiency to be dispersed in water and therefore resulted in a low yield for the formation of COF-301. We also utilized palmitic acid ($CH_3(CH_2)_{14}COOH$) for the synthesis. It led to clusters with a yield of 81% (Extended Data Fig. 4b), indicating the glycine group played a crucial role in keeping COF-301 in well-defined shapes and as monodispersed particles. We further synthesized palmitoyl-*L*-alanine (C_{16}-*L*-AlaA), palmitoyl-*L*-phenylalanine (C_{16}-*L*-PhalaA), palmitoyl-*L*-valine (C_{16}-*L*-ValA) and (S)-3,3-dimethyl-2-palmitamidobutanoic acid (C_{16}-*L*-*t*LeuA) (see Supplementary Information Section 1.1 for details) to investigate the effects of steric hindrance near the polar groups of the amino-acid derivatives on the morphology, size and yield, and no significant difference was observed (Extended Data Fig. 4c).

Control experiment without adding PTSA led to disordered materials with a yield of 5% (Extended Data Fig. 5). The yield of single-crystal COF-301 increased with the increase of molar concentration of PTSA, reached maximum at six equivalent molar amounts to linker-A, and slightly fluctuated thereafter. Meanwhile, the time needed for achieving pure crystals decreased and shortened to 3 days at 9 and 10 molar equivalents of PTSA (Extended Data Fig. 5). Acetic acid and hydrogen chloride were also utilized as catalysts, and they provided lower yield (Extended Data Fig. 6). Interestingly, hydrogen chloride could offer larger crystals than that with PTSA. This can be attributed to the stronger acidity of hydrogen chloride, which facilitates the hydrolysis of the disordered polyimines into monomers and dimers as building units for subsequent crystal growth.

This biomimetic synthesis strategy shows general applicability. We chose monomers with parent core (terephthalaldehyde (linker-B)), electron-accepting (2,3,5,6-tetrafluoroterephthalaldehyde (linker-C)), heterocyclic (pyridine-2,5-dicarbaldehyde (linker-D)) besides the electron-donating (linker-A) substitutions near aldehyde groups and monomers with different length (4,4'-biphenyldicarboxaldehyde, linker-E) to gain single-crystal COF-300, SYSU-8, SYSU-9 and COF-320 under the same crystallization condition as the synthesis of COF-301 (Methods). Single-crystal and mono-dispersed COFs were obtained in all cases (Fig. 1h, i and Extended Data Fig. 7a, b), though the substitutions can notably affect the reaction activity of aldehyde groups and the crystallization process[11]. This is in sharp contrast to the contemporary synthesis methods for COFs, such as the solvothermal method, which requires extensive refinement of optimal reaction conditions on minor change in the monomer structure[10] (see Supplementary Information Section 1.2 for details). All non-hydrogen atoms of the crystals were identified (Fig. 3c-3f and see Supplementary Information Section 2, 3 for details). The typical size of as-synthesized SYSU-9 (termed as SYSU-9-S) was ~ 20 μm × 3 μm (Fig. 1h), and its structure was determined by single-crystal XRD with a resolution of 1.1 Å (Fig.3e). SYSU-9-S crystallized in the space group $I4_1$ (a = 26.461(4) Å, c = 7.4600(15) Å). The size of SYSU-8 was ~ 15 μm × 3 μm (Fig. 1i). COF-320 crystallized in the space group $I4_1/a$ (a = 23.360 Å, c = 8.430 Å) and an interpenetration degree of 9-fold (Fig. 3f). A new crystal phase was obtained, its symmetry was higher than that synthesized by solvothermal method [24], and allowed atomic structure by continuous rotation electron diffraction with an increased resolution of ~ 0.9 Å (see Supplementary Information Section 2 for details). The size of COF-300 could be down to 600 nm (see Supplementary Information Section 1.3 for details) which made it processable as colloids, for example, into flexible films (Extended Data Fig. 8). All the synthesized COFs have one-dimensional (1D) straight channels in which the substitutions distributed spirally, offering varied channel surfaces with different polarity and pore size (COF-301-W: 3.1 Å; COF-300: 5.5 Å; SYSU-8: 5.0 Å; SYSU-9-W: 6.8 Å, COF-320: 6.7 Å) (Fig. 3b-f). We then chose 2DCOF-TTA-TBA as an illustrative example to extend the biomimetic synthesis methodology to synthesize organic 2D materials due to their great potential to go beyond inorganic analogues such as graphene and MoS_2 and great potential as key materials for next-generation technologies[25]. AA stacked nanosheets with the space group *P-6* (a = 17.875 (8) Å, c = 3.4652 (11) Å) were obtained (Extended Data Fig. 7c and see Supplementary Information Section 3 for details). Its thickness was about 50 nm, and could be easily dispersed well in solvents such as water and filtered into thin films (Extended Data Fig. 8). Importantly, the sheets could also be exfoliated by sonication into nanosheets with a thickness down to around 0.7 nm, which corresponded to around 2 layers (Extended Data Fig. 8e). The formation of the imine bonds in all the crystals were also confirmed by solid-state ^{13}C cross-polarization magic angle spinning NMR, FTIR spectroscopy and thermogravimetric analysis (TGA), and permanent porosity of the COFs was confirmed by gas adsorption (see Supplementary Information Section 4-7 for details). By comparing the 77 K nitrogen adsorption of known COFs, COF-300 and COF-TTA-BTA, the biomimetic strategy offered materials (COF-300: 1320 $cm^2\ g^{-1}$; COF-TTA-BTA: 1438 $cm^2\ g^{-1}$) with Brunauer-Emmett-Teller surface area slightly higher than best reported results from COFs obtained with contemporary methods.[26, 27] (Extended Data Fig. 9).

The C_{16}-*L*-*t*LeuA could also be spread on the water surface to induce the crystallization of COF-366 (Methods), a typical 2D COF [28]. Initially, amorphous films were formed and stabilized underneath C_{16}-*L*-*t*LeuA (Extended Data Fig. 9), and gradually transformed into crystalline film with micrometer-sized single-crystal domains. The high crystallinity of the domain enabled near-atomic structure observation by aberration-corrected high-resolution TEM with a resolution down to ~ 2 Å (Extended Data Fig. 10).

We further investigated the role of the pore structure and pore wall structure in tuning the porosity of the single-crystal COFs with adsorption of CO_2 at 195K and 273K (Fig. 4a, 4b). In the uptake of CO_2, 'gate type' sorption profile occurred at 195 K[29], and disappeared at 273K. The gate opening pressure at which an abrupt increase in adsorption after a threshold pressure and the uptake of CO_2 could be tuned by varying the pore surface or adsorption temperature, allowing systematic controlling of the uptake. Among them, COF-300 offered a CO_2 uptake of 480 and 8.5 $cm^3\ g^{-1}$ (P/P_0 = 0.95) at 195K and 273K, respectively (Fig. 4a, b). Interestingly, the substitutions applied to COF-300 (P/P_0 = 0.95) significantly decreased the uptake at 195K, while increased by 294%, 384%, 624%, and 729% with COF-320 (25 $cm^3\ g^{-1}$), SYSU-8 (30 $cm^3\ g^{-1}$), COF-301 (53 $cm^3\ g^{-1}$), and SYSU-9 (62 $cm^3\ g^{-1}$) at 273K, respectively.

A key obstacle in exploring the application of single-crystal COFs is mass production, which remains challenging to be resolved[30]. We demonstrated the capability of scale-up of the biomimetic strategy with gram-scale production of single crystals of COF-301 (yield = 92%), COF-300 (yield = 95%), SYSU-8 (yield = 94%), SYSU-9 (yield = 93%), COF-320 (yield = 94%) and COF-TTA-BTA (yield = 92%) (Fig. 4c, d). In contrast, the yield of single-crystal COF-300 has been reported, which amounted to 49.8% [12]. Importantly, the amino-acid derivatives could be recovered by recrystallization with a recovering rate of ≥ 92%.

In summary, we developed a new path and strategy for crystal growth of organic polymers, revealed the formation mechanism and crystal growth model, and presented the production of six types of single-crystals COFs with controlled size, compositions and properties at the gram-scale besides a two-dimensional COF in water under ambient conditions.

Declarations

Data availability

All data supporting the findings of this study are available within the paper and its Supplementary Information files. Additionally, the X-ray crystallographic coordinates for structures of C_{16}-*L*-*t*LeuA, COF-301-S and SYSU-9-S have been deposited at the Cambridge Crystallographic Data Centre (CCDC), under deposition numbers of CCDC 2049342, CCDC 2209466 and CCDC 2049378, respectively.

Acknowledgements

We thank financial support from National Natural Science Foundation of China (52061135103, 52173296, 21871009 and 22125102). Structure characterizations were supported by Instrumental

Analysis and Research Center of Sun Yat-sen University and Institute of Chemistry, Chinese Academy of Sciences, Diamond Light Source (Didcot, UK). We thank Y. N. Fan for access to powder XRD and FT-IR, S. Y. Guan for access to NMR, X. H. Zhu for access to ESI-HRMS, and J. Li and S. A. Sapchenko for help with data collection of some materials.

Author contributions

ZK. Z. initiated the project. ZK. Z. and W. L. coordinated the research. ZK. Z. and ZP. Z. designed the experiments. ZP. Z. performed most of the experimental work. L. Z., P. C. and J. S. performed cRED, and atomic structure analysis. Y. Y., Y. L. and F. T. helped with the synthesis. H. W., Y. Q. and X. D. carried out TEM and SAED. L. G. and Z. L. conducted AFM. I. Y. and S. Y. conducted synchrotron radiation single-crystal XRD. Y. H. and X. D. helped with the PXRD analysis. P. C. carried out the high resolution PXRD measurements. J. Y. and C. W. measured N_2 and CO_2 adsorption-desorption experiments. ZK. Z., ZP. Z., J. S., L. Z., W. L, and H. Q wrote the manuscript. All authors contributed to the proofreading of the manuscript.

Competing interests

The authors declare no competing interests.

Additional information

Supplementary information

Correspondence and requests for materials should be addressed to liuw226@mail.sysu.edu.cn; junliang.sun@pku.edu.cn; zhengzhikun@mail.sysu.edu.cn

References

1. Simpson, T. L. & Volcani, B. E. *Silicon and siliceous structures in biological systems* (Springer, New York, 1981).
2. Lowenstam, H. A. Minerals formed by organisms. *Science* **211,** 1126–1130 (1981).
3. Kahil, K. et al. Cellular pathways of calcium transport and concentration toward mineral formation in sea urchin larvae. *PNAS* **117**, 30957-30965 (2020).
4. Gower, L. B. et al. Biomimetic model systems for investigating the amorphous precursor pathway and its role in biomineralization. *Chem. Rev.* **108**, 4551–4627 (2008).
5. Sommerdijk, N. & With, G. de Biomimetic $CaCO_3$ mineralization using designer molecules and interfaces. *Chem. Rev.* **108**, 4499–4550 (2008).
6. Côté, A. P. et al. Porous, Crystalline, Covalent Organic Frameworks. *Science* **310**, 1166-1170 (2005).

7. Peng, L., Guo, Q., Song, C. et al. Ultra-fast single-crystal polymerization of large-sized covalent organic frameworks. *Nat. Commun.* **12**, 5077 (2021).
8. Geng, K. Y. et al. Covalent organic frameworks: Design, synthesis, and functions. *Chem. Rev.* **120**, 16, 8814–8933 (2020).
9. Smith, B. J. Overholts, Hwang, A. C. N. & Dichtel, W. R. Insight into the crystallization of amorphous imine-linked polymer networks to 2D covalent organic frameworks. *Chem. Commun.* **52**, 3690-3693 (2016).
10. Smith, B. J. & Dichtel, W. R. Mechanistic studies of 2D covalent organic frameworks rapidly polymerized from initially homogenous conditions. *J. Am. Chem. Soc.* **136**, 8783-8789 (2014).
11. Ma, T. Q. et al. Single-crystal x-ray diffraction structures of covalent organic frameworks. *Science* **361**, 48–52 (2018).
12. Evans, A. M. et al. Seeded growth of single-crystal two-dimensional covalent organic frameworks. *Science* **361**, 52–57 (2018).
13. Sakai, N. & Matile, S. Conjugated polyimine dynamers as phase-sensitive membrane probes. *J. Am. Chem. Soc.* **140**, 11438–11443 (2018).
14. Li, Z. et al. Structural and Dimensional transformations between covalent organic frameworks via linker exchange. *Macromolecules* **52**, 1257–1265 (2019).
15. Pramudya, Y. & Mendoza-Cortes, J. L. Design principles for high H_2 storage using chelation of abundant transition metals in covalent organic frameworks for 0-700 bar at 298K. *J. Am. Chem. Soc.* **138**, 15204–15213 (2016).
16. Pritula, I. & Sangwal, K. *Fundamentals of Crystal Growth from Solutions. Handbook of Crystal Growth: Bulk Crystal Growth Ed. P. Rudolph, 2nd ed.* (Elsevier, 2015, pp. 1185–1227).
17. Markov, I. V. *Crystal Growth and Epitaxy, Crystal Growth for Beginners: Fundamentals of Nucleation* (World Scientific, Singapore, 2016).
18. Lovette, M. A. et al. Crystal shape engineering. *Ind. Eng. Chem. Res.* **47**, 9812–9833 (2008).
19. Olafson et al. Early onset of kinetic roughening due to a finite step width in hematin crystallization. *Phys. Rev. Lett.* **119**, 198101 (2017).
20. Ulrich, J. & Bülau, H. C. *Melt crystallization. Handbook of Crystal Growth, 2nd ed.* (Elsevier, 2002, pp. 161–179).
21. Zhan, G. L. et al. Observing polymerization in 2D dynamic covalent polymers. *Nature* **603**, 835-840 (2022).
22. Kissel, P. et al. A nanoporous two-dimensional polymer by single-crystal-to-single-crystal photopolymerization. *Nat. Chem.* **6**, 774-778 (2014).
23. Pal, A. et al. Molecular mechanism of physical gelation of hydrocarbons by fatty acid amides of natural amino acids. *Tetrahedron* **63**, 7334–7348 (2007).
24. Zhang, Y. B. et al. Single-crystal structure of a covalent organic framework. *J. Am. Chem. Soc.***135**, 16336-16339 (2013).

25. Feng, X. L. & Schlüter, A. D. Towards macroscopic crystalline 2D polymers. *Angew. Chem. Int. Ed.* **57**, 13748–13763 (2018).
26. Ma, T. Q. et al. Observation of interpenetration isomerism in covalent organic frameworks. *J. Am. Chem. Soc.***140**, 6763–6766 (2018).
27. Zhao, W. et al. Using sound to synthesize covalent organic frameworks in water *Nature Synthesis.* **1**, 87-95 (2022).
28. Lin, S. et al. Covalent organic frameworks comprising cobalt porphyrins for catalytic CO_2 reduction in water. *Science*, 349, 1208-1213 (2015).
29. Horike, S., Shimomura, S. & Kitagawa, S. Soft porous crystals. *Nat. Chem.* **1**, 695-704 (2009).
30. Peng, Y. W. et al. Room temperature batch and continuous flow synthesis of water-stable covalent organic frameworks (COFs). *Chem. Mater.* **28**, 5095–5101 (2016).

Methods

Synthesis procedures of single-crystal COFs

General procedure A: To grow the single-crystal COFs, we dissolved 0.1 mmol amino-acid derivatives (C_8-GlyA, C_{10}-GlyA, C_{12}-GlyA, C_{14}-GlyA, C_{16}-GlyA, C_{18}-GlyA, C_{16}-*L*-AlaA, C_{16}-*L*-PhalaA, C_{16}-*L*-ValA or C_{16}-*L*-*t*LeuA) and 0.1 mmol sodium hydroxide in 8.5 mL of water at 50 ℃ under ambient conditions. The solution was stirred for 10 minutes to obtain an emulsion of uniform size, then 0.05 mmol (linker-A/B/C/D/E) was added and stirred. Subsequently, a solution of tetrakis(4-aminophenyl)methane (TAM, 9.5 mg, 0.025 mmol) in 0.2 mol L^{-1} acid (PTSA/HCl/HOAc, 1.5 mL) was added, stirred for 5 minutes. After the completion of the reaction, the product was collected by centrifugation and washed three times with water and tetrahydrofuran. Further purification of COFs was carried out by immersing in tetrahydrofuran for 24 hours, dried at ambient temperature for 12 hours and 100 ℃ for 12 hours to afford single-crystal COFs powder.

Gram-scale production of COF-301/301, SYSU-8 and SYSU-9 was performed by parallel increase of the molar amounts of added chemicals and volume of reactors:

C_{16}-GlyA (3.134 g, 10 mmol) and linker-A (0.831 g, 5 mmol) were explored to gain COF-301 (Yield: 92%, 1.48 g) *under general procedure A*. Recovering rate of C_{16}-GlyA: 93%, 2.91 g.

C_{16}-GlyA (3.134 g, 10 mmol) and linker-B (0.671 g, 5 mmol) were explored to gain COF-300 (Yield: 95%, 1.37 g) *under general procedure A*. Recovering rate of C_{16}-GlyA: 96%, 3.01 g;

C_{16}-GlyA (3.134 g, 10 mmol) and linker-C (1.030 g, 5 mmol) were explored to SYSU-8 (Yield: 94%, 1.69 g) *under general procedure A*. Recovering rate of C_{16}-GlyA: 97%, 3.03 g;

C_{16}-GlyA (3.134 g, 10 mmol) and linker-D (0.676 g, 5 mmol) were explored to gain SYSU-9 (Yield: 93%, 1.35 g) *under general procedure A*. Recovering rate of C_{16}-GlyA: 92%, 2.88 g.

C_{16}-GlyA (3.134 g, 10 mmol) and linker-E (1.051 g, 5 mmol) were explored to gain COF-320 (Yield: 94%, 1.72 g) *under general procedure A*. Recovering rate of C_{16}-GlyA: 92%, 2.88 g.

Synthesis procedures of 2DCOF-TTA-BTA

To grow the 2D COFs, we dissolved 0.1 mmol C_{16}-*L*-ValA and 0.1 mmol sodium hydroxide in 10 mL of water. Stir at 50 ℃ for 10 minutes to obtain an emulsion of uniform size, then benzene-1,3,5-tricarbaldehyde (BTA, 4.1 mg, 0.025 mmol) was added and stirred. Then a solution of 4,4',4"-(1,3,5-triazine-2,4,6-triyl)trianiline (TTA, 8.85 mg, 0.025 mmol) in 0.2 mol L^{-1} PTSA (1.5 mL) was added, stirred for 5 minutes. After the completion of the reaction, the product was collected by centrifugation and washed three times with water and tetrahydrofuran. Further purification of COFs was carried out by immersing in tetrahydrofuran for 24 hours, dried at ambient temperature for 12 hours and 100 ℃ for 12 hours to afford 2DCOF-TTA-BTA powder. **Gram-scale production:** C_{16}-*L*-ValA (3.556 g, 10 mmol), TTA (885 g, 2.5 mmol) and BTA (410 g, 2.5 mmol) were explored to gain highly crystalline 2DCOF-TTA-BTA powder (Yield: 92%, 1.07 g). Recovering rate of C_{16}-*L*-ValA: 92%, 3.27 g.

Synthesis procedures of single-crystal COF-366

P-toluenesulfonic acid monohydrate (PTSA)was dissolved in water to prepare 2 mol L^{-1} PTSA aqueous solutions. Then 5,10,15,20-Tetrakis (4-aminophenyl)-21H,23H-porphyrin (TAPP) was dissolved in 2 mol L^{-1} PTSA solution to prepare 1 mg mL^{-1} TAPP solution. 2,5-Dihydroxyterephthalaldehyde is dissolved in ethylene glycol solution to prepare 1mg mL^{-1} 2,5-Ph solution. All solutions are sonicated for 30 minutes prior to use.

In a general synthetic procedure 25 mL water was added in a petri dish with a diameter of 56 mm and a height of 16 mm. An ethanol solution of C_{16}-*L*-*t*LeuA (60 µL, 1 mg mL^{-1}) was spread at the air-water interface and left undisturbed for 30 minutes. Solution of TAPP protonated with 2 mol L^{-1} PTSA (200 µL, 0.3 µmol) was added to the petri dish and left undisturbed for 60 minutes. Then, the aqueous solution of aldehyde monomers was slowly injected into the container. Single-crystal COF-366 were obtained after one week. The films were then transferred onto substrates of interest from the air-water surface and cleaned with water and chloroform before characterization.

Figures

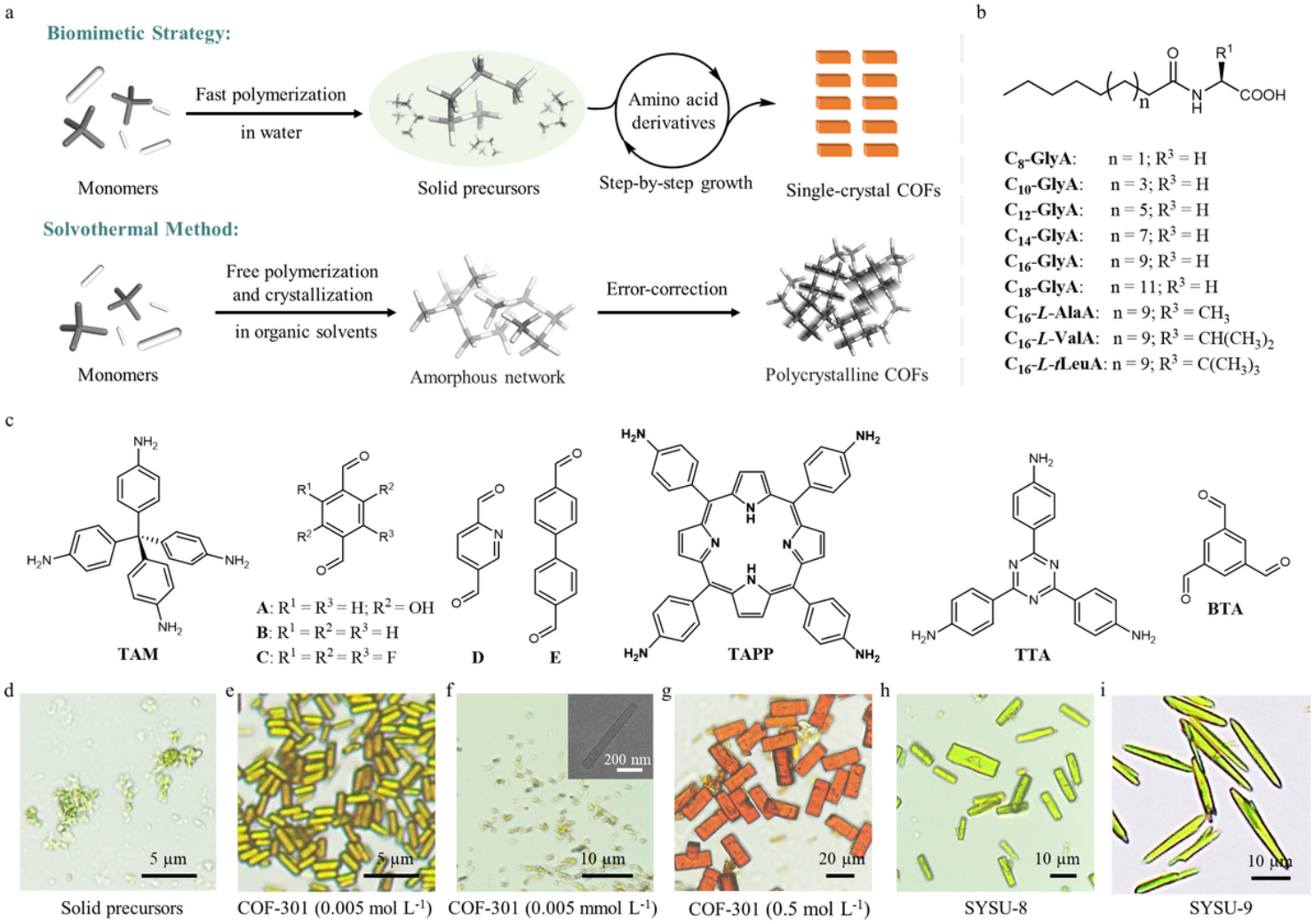

Figure 1

Synthesis protocol and morphology of COFs. a, Schematic view of the biomimetic growth and traditional solvothermal method to create single-crystal COFs. **b**, amphiphilic molecules of amino acid derivatives (**b**), **c**, chemical structure of tetrakis(4-aminophenyl)methane (TAM), linker-A to linker-E, 5,10,15,20-Tetrakis (4-aminophenyl)-21H,23H-porphyrin (TAPP), monomer 4,4',4"-(1,3,5-triazine-2,4,6-triyl)trianiline (TTA), monomer benzene-1,3,5-tricarbaldehyde (BTA) **d-i**, Optical microscopy and scanning electron microscope (SEM) images of the synthesized products under mediation of C_{16}-GlyA in water under ambient conditions (COF-301: TAM and linker-A; SYSU-8: TAM and linker-C; SYSU-9: TAM and linker-D).

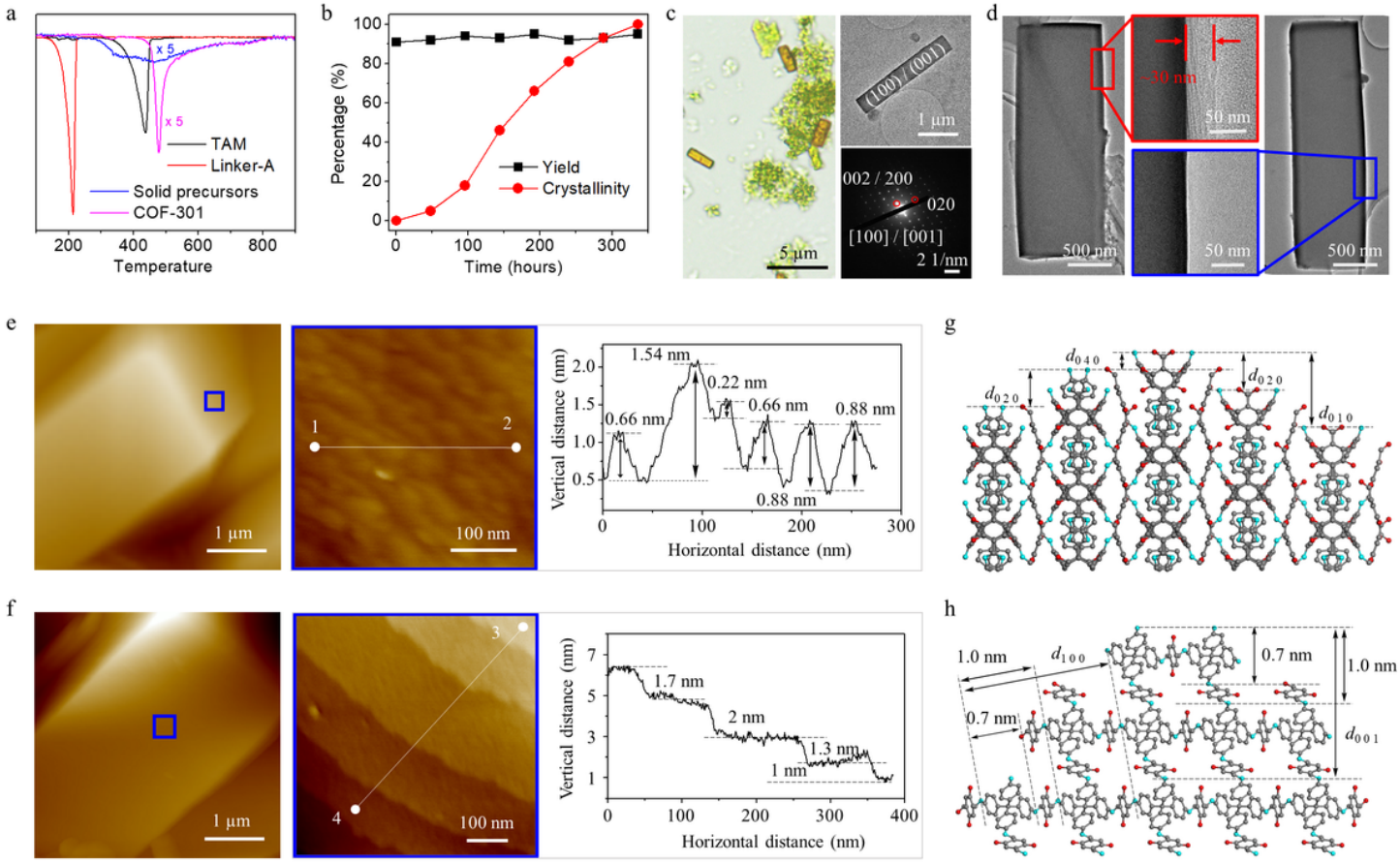

Figure 2

Growth mechanism of single-crystal COF-301. a, Derivative Thermogravimetry (DTG) of solid precursorsand COF-301. **b**, The evolution of the percentage of the yield and crystallinity of reaction products over time. **c**, The product at day two contained both amorphous materials and COF-301. **d**, Transmission electron microscopy images show the morphology of the crystals in the reaction system (left) before and (right) after cleaning with tetrahydrofuran. **e**, **f**, Atomic force microscopy (AFM) topographic images of the growing (0 1 0) (**e**) and (1 0 0)/ (0 0 1) facets (**f**) after being rinsed with tetrahydrofuran and dried in air. **g**, **h**, The structure viewed along the ***a*** axis (**g**) and ***b*** axis (**h**) direction of the COF-301-W.

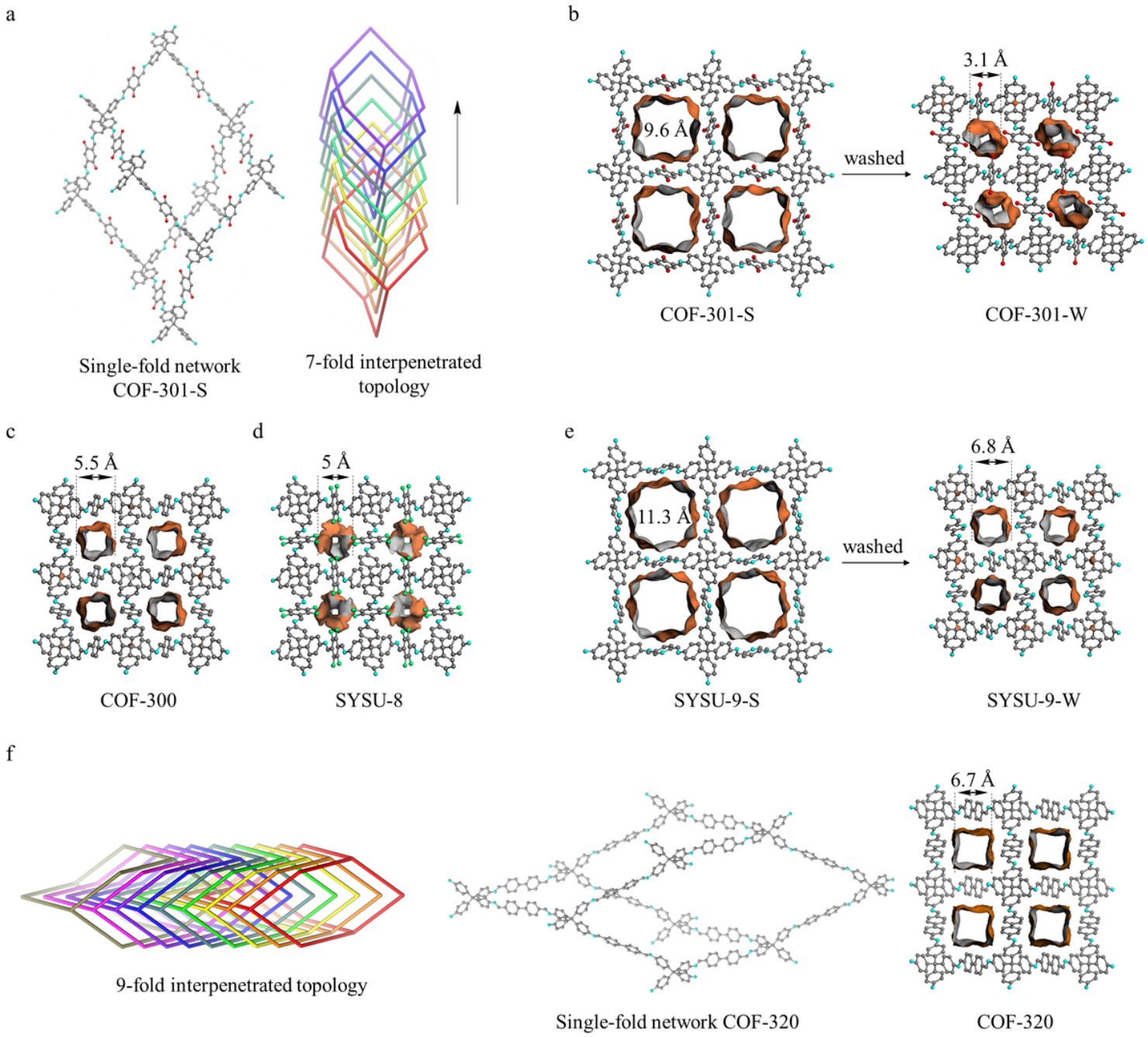

Figure 3

Single-crystal structure of COFs. a, Single-fold diamond (*dia*) network and the 7-fold interpenetrated *dia* topology of COF-301-S. **b**, Structures of COF-301-S and COF-301-W. **c**, **d**, The structures of COF-300 (**c**), and SYSU-8 (**d**). **e**, Structure of SYSU-9 (termed as SYSU-9-S) before and after washing (termed as SYSU-9-W) with tetrahydrofuran. **f**, Single-fold diamond (*dia*) network and the 9-fold interpenetrated *dia* topology of COF-320. Atoms of carbon are shown in grey, nitrogen in blue, oxygen in red, and fluorine in green. Disordered guest molecules within the pores are omitted for clarity.

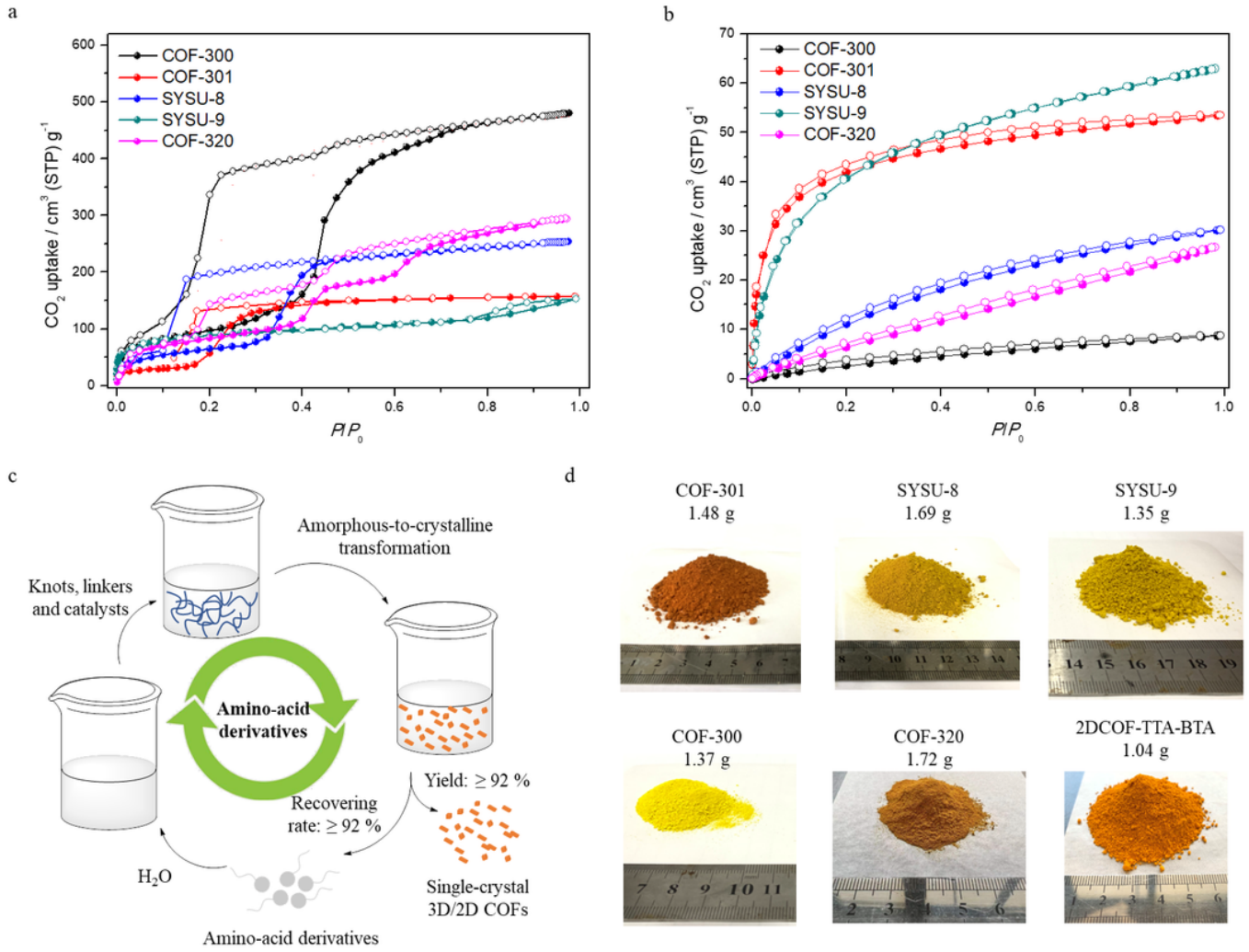

Figure 4

Scale-up production of single-crystal COFs. a, CO_2 adsorption isotherm of COF-300, COF-301, SYSU-8/9 and COF-320 at 195 K. **b**, CO_2 adsorption isotherm of COF-300, COF-301, SYSU-8/9 and COF-320 at 273K. **c**, Schematic view of mass production of single-crystal COFs. **d**, Photographic demonstration of gram-scale synthesis.

Supplementary Files

This is a list of supplementary files associated with this preprint. Click to download.

- ZZPSupplementaryInformation20220927.docx
- ExtendedDataFigures.docx